ISSN 1024-8560, Atmospheric and Oceanic Optics, 2024, Vol. 37, No. 6, pp. 911–918. © Pleiades Publishing, Ltd., 2024.
Russian Text © The Author(s), 2024, published in Optika Atmosfery i Okeana.

OPTICAL INSTRUMENTATION

Airborne Lidar BSE-6 for Remote Detection of Clear-Air Turbulence

B. D. Belan[a], I. A. Razenkov[a, *], and K. A. Rynkov[a]

[a] *V.E. Zuev Institute of Atmospheric Optics, Siberian Branch, Russian Academy of Sciences, Tomsk, 634055 Russia*

**e-mail: lidaroff@iao.ru*

Received April 23, 2024; revised June 18, 2024; accepted June 19, 2024

Abstract—The development of instruments for remote detection of clear-air turbulence (CAT) for early warning of aircraft crew about the danger is an urgent problem today. In this work, we describe the design and technical features of BSE-6 turbulent lidar mounted onboard an aircraft for experimental testing of CAT remote sensing technique. The quality of assembly and adjustment was verified in comparison between theoretical calculations and real echo signals. The system was tested for thermomechanical stability. The improvement of the turbulent lidar is to ensure early detection of CAT from an aircraft and remote control of the turbulence intensity in the atmospheric boundary layer from the ground, for example, along glide paths at airports.

Keywords: turbulent lidar, backscatter enhancement effect, clear-air turbulence, aviation safety

DOI: 10.1134/S1024856024701173

INTRODUCTION

According to the International Civil Aviation Organization, the primary cause of aviation accidents is turbulence, when an aircraft experiences severe turbulence and can become temporarily uncontrollable [1, 2]. Clear air turbulence (CAT) suddenly occurs in the upper troposphere in jet stream zones at altitudes from 6 to 12 km. In contrast to other turbulence types, it is not accompanied by significant clouds. Visual detect of CAT is difficult because of the lack of obvious signs. Airborne weather radars only detect echo signals from large aerosol particles, and, hence, ignore CAT. Today, the problem of remote detection of CAT for early warning of aircraft crew is relevant and requires a solution.

The technique for optical sounding of CAT by laser locators (lidars) seems promising, and such experience already exists. For example, CAT were successfully remotely detected with an infrared Doppler lidar by the Japan Aerospace Exploration Agency (JAXA) [3, 4]. A laser system the operating principle of which is based on the backscatter enhancement effect (BSE) in the visible or ultraviolet (UV) spectral regions can be an alternative to Doppler lidars [5, 6].

A turbulent lidar is a specialized micropulse aerosol eye-safe optical locator with two receiving channels [7]. The lidar simultaneously implements two transceiver design schemes: coaxial (the main transceiving channel) and biaxial (additional receiving channel) [8, 9]. The first channel is main, it is combined with the transmitting channel; the second channel is additional and is located next to the main one. The additional receiving channel records lidar echoes from molecules and aerosol particles. Echoes of the main channel differs from those of the additional channel only by the turbulent component, which is caused by an increase in backscattering. The BSE component in an echo signal is the result of a double propagation of a light wave through a random medium, and its magnitude is proportional to the turbulence [10]. The optical turbulence intensity profile along the sounding direction is estimated from the ratio of the main and additional echoes. The turbulent lidar sounding technique is described in detail in [11].

In September 2022, the first results of turbulence sounding with BSE-5 UV lidar from a Tu-134 aircraft were received, which made it possible to record changes in the structural characteristics of turbulent fluctuations in air refractive index C_n^2 at an altitude of 9 km and distances of up to 8 km [12]. The sounding was carried out perpendicular to the aircraft fuselage. During the four-hour flight, C_n^2 changed by more than an order of magnitude while passing through turbulent zones. In May 2024, Chaplygin Siberian Scientific Research Institute of Aviation modified and certified emergency exit hatch of Tu-134 aircraft, which is to enable sounding in the flight direction.

The aim of this work was to design BSE-6 turbulent lidar for mounting onboard Tu-134 aircraft laboratory.

1. LIDAR DESIGN

There are two possible design options for transceiving optics of a turbulent lidar: with one large telescope like in BSE-5 lidar or with two small telescopes like in BSE-4 lidar [7]. In the first case, the system is easier to

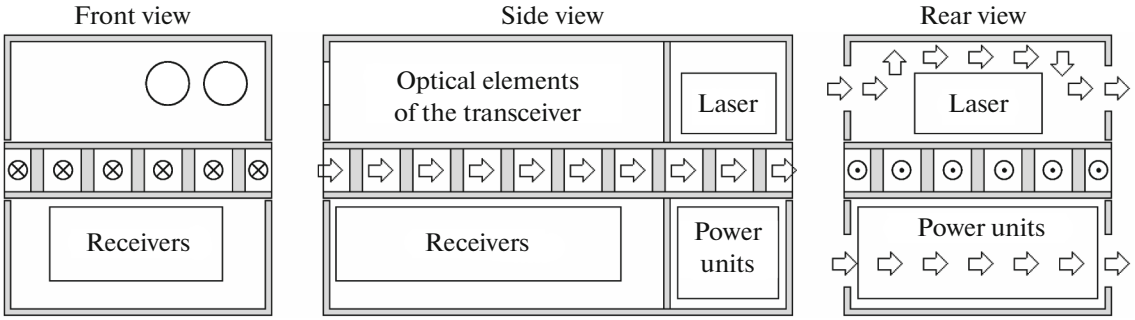

Fig. 1. Design concept of airborne turbulence lidar. The arrows show the direction of air flow through the optical bench (in the center) and the sections with the laser and power supplies (on the right).

adjust, but larger. A version with two telescopes was chosen to reduce the system size and weight.

During the work, recommendations suggested in [7] were taken into account in order to create a compact and thermomechanically stable design independent of variations in the outside temperature. To reduce the size of the lidar, it was decided to use both sides of an optical bench mounting a transceiver on one side and the receiving part with photodetectors on the other side (Fig. 1).

To reduce the temperature gradient between the sides of the optical bench, outside air was pumped through the middle of the bench. An optical bench typically consists of a pair of aluminum plates connected by multiple aluminum bushings, which makes it light and rigid. It was decided to place all heat-generating elements, such as a laser and power supplies, in isolated sections and to provide outside air pumped through them for cooling [7]. At the point where light beams pass through the optical bench, it is necessary to mount a dust-proof channel (not shown in Fig. 1).

The optical diagram of the lidar is shown in Fig. 2. The transceiver is assembled on side *1* of the optical bench, and the receiving module and power supplies are mounted on side *2*. Beam *4* (shown by arrows) from laser *3* is guided to a 10× afocal telescope 50 mm diameter by turning mirrors *5–7* and thin-film polarizer *9*. The telescope consists of off-axis parabolic mirrors *12* and *13* (Mersenne). Fig. 2a shows collimating lens *8* and quarter-wave plate *11* which transforms linearly polarized laser radiation into circularly polarized one. Telescope *12–13* 10-fold expands beam *4* and sends it into the atmosphere. Thin film polarizer *9* and quarter-wave plate *11* form an antenna switch which redirects light beams arriving from the atmosphere to receiving module *32*. Element *10* in the diagram is a structure for fastening optical fiber through which part of laser radiation is transmitted to the photon counter as a synchronization signal.

Main *15* and additional *16* beams (marked with arrows) are guided to the telescopes consisting of mirrors *12* and *13* (main transceiving channel) and *18* and *19* (additional receiving channel), respectively. Mirrors *18* and *19* are identical to mirrors *12* and *13*. Elements *14* and *17* are antireflected wedge-shaped windows. Beams *15* and *16* are oriented parallel to each other by mirrors *20* and *21* and are directed to receiving module *32* by turning mirrors *22–24*.

Interference filter *25* is mounted at the entrance to module *32*. Next, a spatial filter is fixed which determines the field-of-view of the receiver and consists of focusing *26* and collimating *28* lenses and aperture stop *27*. Beam *15* of the main receiving channel is directed to detector *31* by elliptical turning mirror *30*, and beam *16* of the additional channel is directed to detector *29*. Laser *3* and power supplies *33* and *34* are located in ventilated isolated sections on opposite sides of the optical bench. Fig. 3 shows the lidar model, the transceiver, and the appearance of BSE-6 lidar. The lidar parameters are tabulated.

The transceiver is mounted in an aluminum frame (Fig. 3c). It is vertically arranged due to the shape and size of the fairing located on the outside of the aircraft fuselage. The fairing is equipped with two quartz windows and a rectangular turning mirror, which are also vertical. The frame with the lidar is attached via rubber buffers to the lower frame, where an uninterruptible power supply and an on-board DC (+27 V)-to-AC (~220 V) converter are fixed.

2. LIDAR TRANSCEIVER ALIGNMENT

Adjustment and alignment of complex optical systems is an important stage in their creation. In our case, the alignment procedure has a number of features due to the use of two afocal telescopes consisting of off-axis parabolic mirrors. The alignment tasks included: 1) precise alignment of the focal points of mirrors *12* and *13*, *18* and *19* (Fig. 4) for each telescope; 2) alignment of the telescope axes parallel to each other; 3) alignment of the telescopes parallel to the optical bench.

To perform the alignment, an external 130 m path with a white screen at the end was organized. The lidar was located indoors. Laser *G* (532 nm), an interferometer (shear plate) for monitoring the parallelism of

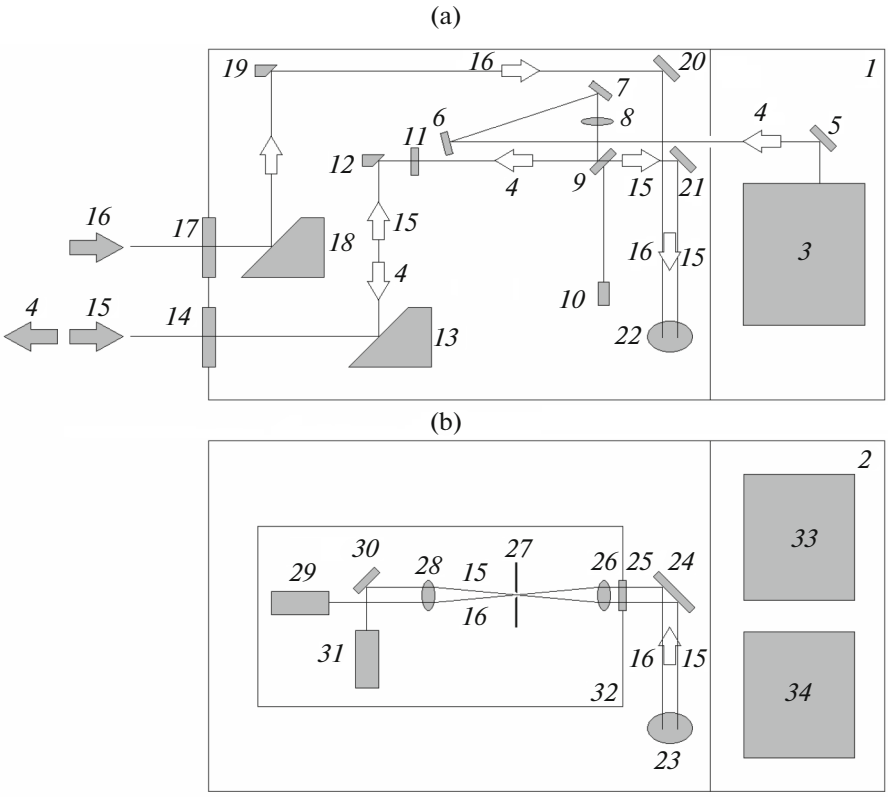

Fig. 2. Optical diagram of BSE-6 lidar: (a) transceiver on side *1* and (b) receiving module on side *2* of the optical bench. See description in the text.

laser beams, retroreflectors (not shown in Fig. 4) and a small telescope were additionally used. Retroreflectors enabled: (1) turning the radiation of the central part of beam *4* of UV laser *3* to 180° in the transmitting channel; (2) redirecting the edge part of beam *4* from the transmitting channel to the second receiving channel.

Figure 4 shows that a visible beam (532 nm) of auxiliary laser *G* is collimated by a positive lens and then sent into the optical bench of the lidar by a pair of mirrors; after that, mirrors *21* and *20* split it in half and beams *A* and *B* are directed to mirrors *12* and *13*, *18* and *19*. Simultaneously, beam *4* of UV laser *3* goes to mirrors *12* and *13*. All three beams are projected onto a screen at a distance of 130 m.

The alignment procedure consisted of collimating visible beams *A* and *B* using an interferometer at the exit from the lidar and combining beams *4* and *A* on the white screen provided that the axes of all beams are parallel and the reflected by the retroreflectors return to the lidar parallel to the optical bench. The left fragment of Fig. 4 shows beam *4* of UV laser *3* and beam *B* of green laser *G* after completion of the alignment procedure. The beams had a Gaussian shape at the exit from the lidar; however it was distorted on the screen (130 m). It was possible that the lidar alignment procedure we used did not provide minimization of the resulting aberrations. To answer the question of whether the alignment result could be considered satisfactory, lidar echoes were theoretically estimated.

3. PHOTON BUDGET AND COMPARISON WITH REAL ECHO SIGNALS

The quality of the lidar assembly and alignment was estimated by comparing the expected result with the actual experiment. For this purpose, lidar echoes were calculated with the use of mirror reflectivity, transmittance of lenses and other optical elements, PMT counting sensitivity, and some other parameters. First, we estimated optical losses inside the lidar during laser energy transmission through the atmosphere and echo signals reception. Then, the lidar echo was calculated by the lidar equation [11] where the model values of the molecular and aerosol scattering coefficients were substituted.

The BSE-6 lidar is equipped with Thorlabs (https://www.thorlabs.com/) and Edmund Optics (https://www.edmundoptics.com/) optical elements. (Manufacturers' data: the reflectivity of mirrors is 0.92 and the transmittance of transparent elements is 0.99). Taking into account the losses on the window glass (0.50) the horizontal-path sounding was performed through, the total transmittance of the transceiver was 0.187.

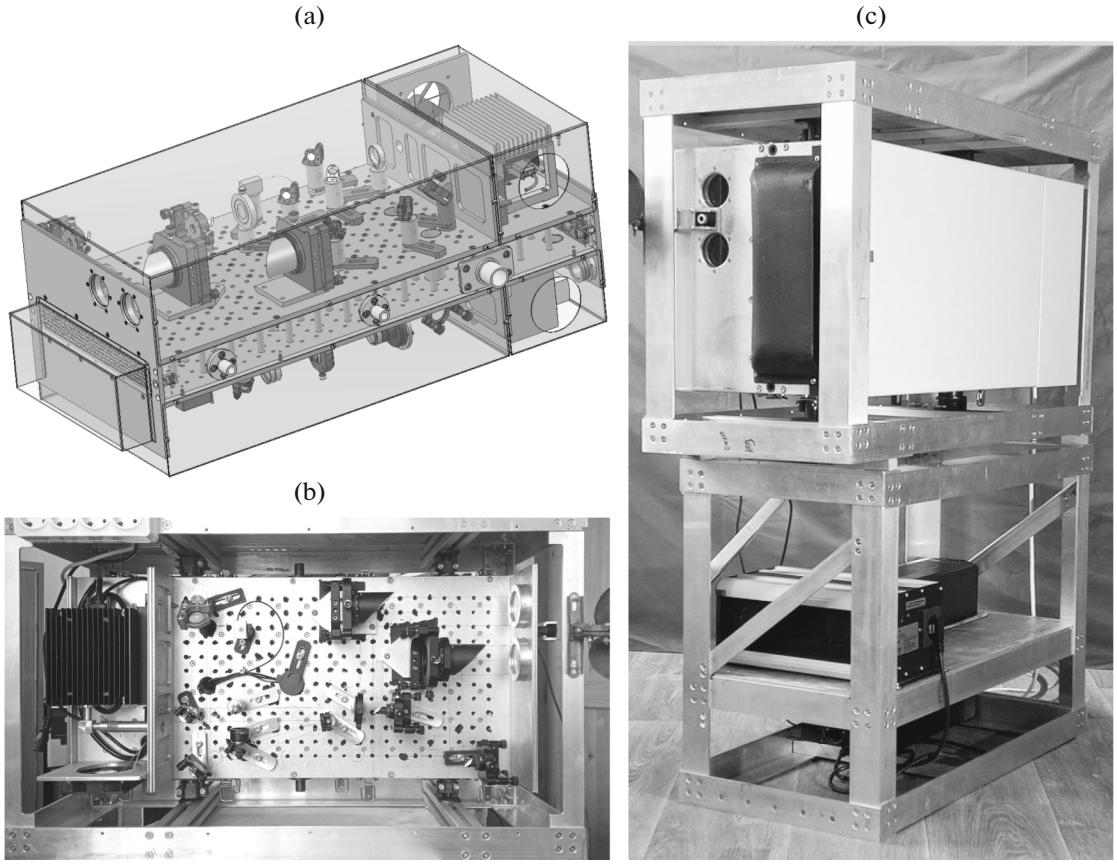

Fig. 3. (a) Model and (b) picture of the transceiver; (c) BSE-6 lidar.

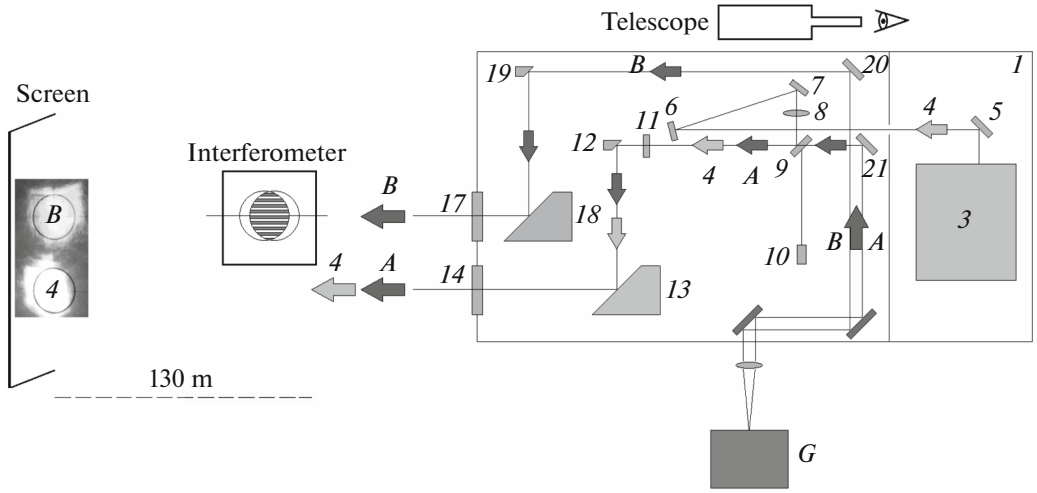

Fig. 4. Lidar alignment diagram. See notations and explanations in the text.

To calculate an echo, the lidar parameters given in Table 1 and the average model scattering coefficients were used. For Rayleigh (molecular) scattering at a wavelength of 355 nm, the following values were taken: scattering coefficient of 0.0071 km^{-1} sr^{-1} and attenuation coefficient of 0.06 km^{-1}. The measurements were carried out in under the clear sky conditions. During measurements, the total attenuation coefficient was estimated at 0.14 km^{-1} from the lidar echoes by the logarithmic derivative method [9]; hence, the aerosol

Table 1. BSE-6 lidar parameters

Parameter	Value
Laser wavelength (Cobolt)	355 nm
Pulse energy	18 μJ
Pulse frequency	7 kHz
Pulse duration	5 ns
Laser output power	125 mW
Laser beam quality	TEM_{00}, $M^2 < 1.3$
Beam diameter at the lidar exit	50 mm
Beam divergence at the lidar exit	20 μrad
Number of telescopes (Mersenne)	2
Distance between telescope axes	85 mm
Telescope diameter	50 mm
Telescope magnification	$10^{\times}$
Field-of-view of receivers	100 μrad
Interference bandpass filter	0.15 nm
Quantum efficiency of PMT (H10682-210P)	33%
Recording technique	Photon counting
Spatial resolution	15 m
Temporal resolution	10 c
Sounding range	10 km
C_n^2 measurement range	10^{-17}–10^{-13} $m^{-2/3}$
Lidar operating mode	Continuous
Operating temperature range	+10...+35°C
Power consumption	Less than 100 W
Overall dimensions L × W × H	1017 × 427 × 446 mm^3
Transceiver weight	50 kg

attenuation coefficient was 0.14–0.06 km^{-1} = 0.08 km^{-1}. The lidar ratio was taken to be 50 sr^{-1}; hence, the aerosol scattering coefficient was 0.0016 km^{-1} sr^{-1}.

The turbulence lidar echoes were calculated in terms of the number of detected photons taking into account a spatial resolution of 15 m (100-ns strobe) and an accumulation interval of 10 s (70000 shots) at an average laser output power of 100 mW. The calculation (curve *1*) and experiment (crosses *2*) results are shown in Fig. 5a. Turbulence was ignored.

The experimental echo was recorded along a near-ground horizontal path under the clear sky conditions. The echo maximum at a distance of 1 km is due to the transceiver geometry. The geometric factor was not taken into account in the calculations; therefore, curve *1* has no maximum.

It is important to compare the results in the far zone. According to Fig. 5a, the calculated echo is twice as large as the actual one up to a distance of 10 km, where the signal-to-noise ratio is higher than 1. One of the reasons for this could be an error in the alignment of the telescopes, which follows from the non-Gaussian shape of the beams in Fig. 4.

Figure 5b shows the echoes calculated for a near-ground horizontal path (curve *1*, 1013 mbar) and a path at an altitude of 10 km (curve *2*, 246 mbar). In the latter calculation, only molecular scattering was taken into account. One can see that the echo near the lidar at an altitude of 10 km is smaller due to the low air density. Starting from a distance of ~10 km, the echo becomes larger due to high air transparency. This means that the theoretical potential of the lidar (sounding range) at an altitude of 10 km is comparable to its potential at the ground level.

4. LIDAR THERMOMECHANICAL STABILITY TESTING

BSE-6 lidar was designed for automatic long-term measurements. Therefore, it was important to ensure the constant the relative positions of the optical axes of the transmitter and receivers. The main reason for

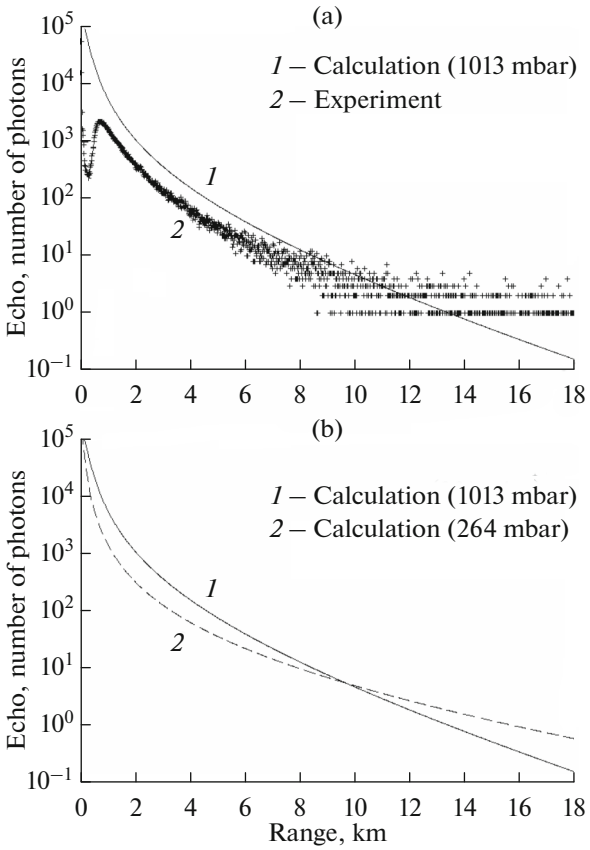

Fig. 5. Theoretical estimation of lidar echoes in comparison with experiment; echo estimates (b) at the ground level (1013 mbar) and (c) at an altitude of 10 km (264 mbar).

possible misalignment of the axes is the deformation of the bend of the optical bench, which occurs in the presence of a temperature gradient between the opposite sides of the bench [7].

The lidar was tested in the normal operation mode during two days in the cold season at an outdoor air temperature of −30°C. At midnight, the circuit breaker turned off the electric heater in the room for 3 h. The room was an insulated veranda; therefore, the temperature inside quickly dropped from +25 to +17°C (Fig. 6).

Figure 6a shows the behavior of the air temperature at the entrance T_1 and exit T_2 of the optical bench. About midday, the room temperature increased by 4°C. In addition, the black light-shielding screen on the front side of the lidar was heated by the sun (the sounding path was directed to the south); hence, temperature T_2 turned out to be lower than temperature T_1 at midday. Figure 6b shows the variation in the temperature on the top (T_3) and bottom (T_4) of the lidar casing. During the day, T_3 increased to +30°C. The curves of the temperature on the top (T_5) and bottom (T_6) sides of the optical bench are shown to be synchronously changing within wide limits from +16 to +26°C in Fig. 6c.

Figure 6d shows the temperature gradient between the bench entrance and exit ($T_2 - T_1$) and its bottom and top ($T_6 - T_5$). One can see that the temperature of the lidar casing changed by 14°C over 48 h. The amplitude of the air flow gradient at the entrance and exit of the bench attained 4°C. The gradient on opposite sides of the optical bench remained near-constant and equal to −0.3°C, increasing to +0.3°C only during the day under direct sunlight.

The experiment showed that if the room temperature is maintained within the range +15...+25°C and the lidar casing is protected from direct sunlight, then the temperature gradient on the bench sides is constant and equal −0.3°C. The constancy of the gradient at the bench sides means its fixed shape and, hence, stable relative position of the optical axes of the transmitter and receivers. Note that changes in the room temperature during the experiment did not affect the sounding results, which also indicated stable behavior of the lidar.

CONCLUSIONS

The concept and design features of BSE-6 turbulent lidar (355 nm) designed for operating onboard an aircraft are described. The lidar is intended for experimental verification of the technique for sounding clear-air turbulence based on the backscatter enhancement effect.

Small size and weight of the lidar are due to the use of both sides of the optical bench. A transceiver is mounted on one side of the bench and a receiving module is mounted on the other side.

The procedure of alignment of afocal lidar telescopes, which consist of off-axis parabolic mirrors, and adjustment of the system as a whole is described. The quality of the lidar alignment and adjustment was estimated from the comparison between real and calculated echoes. The actual signals turned out to be half as large as the calculated ones. A possible reason for this difference is system alignment errors.

Ground-based testing of the lidar for thermomechanical stability showed the temperature gradient on opposite sides of the optical bench in the lidar to be constant and equal to −0.3°C when the room temperature changes from +15 to +25°C. High thermomechanical stabilization of the lidar transceiver was achieved by placing heat-generating elements (laser and power supplies) in individual ventilated sections. BSE-6 lidar is planned to be mounted onboard the Tu-134 “Optic” aircraft laboratory, where it will operate in continuous mode during flight experiments.

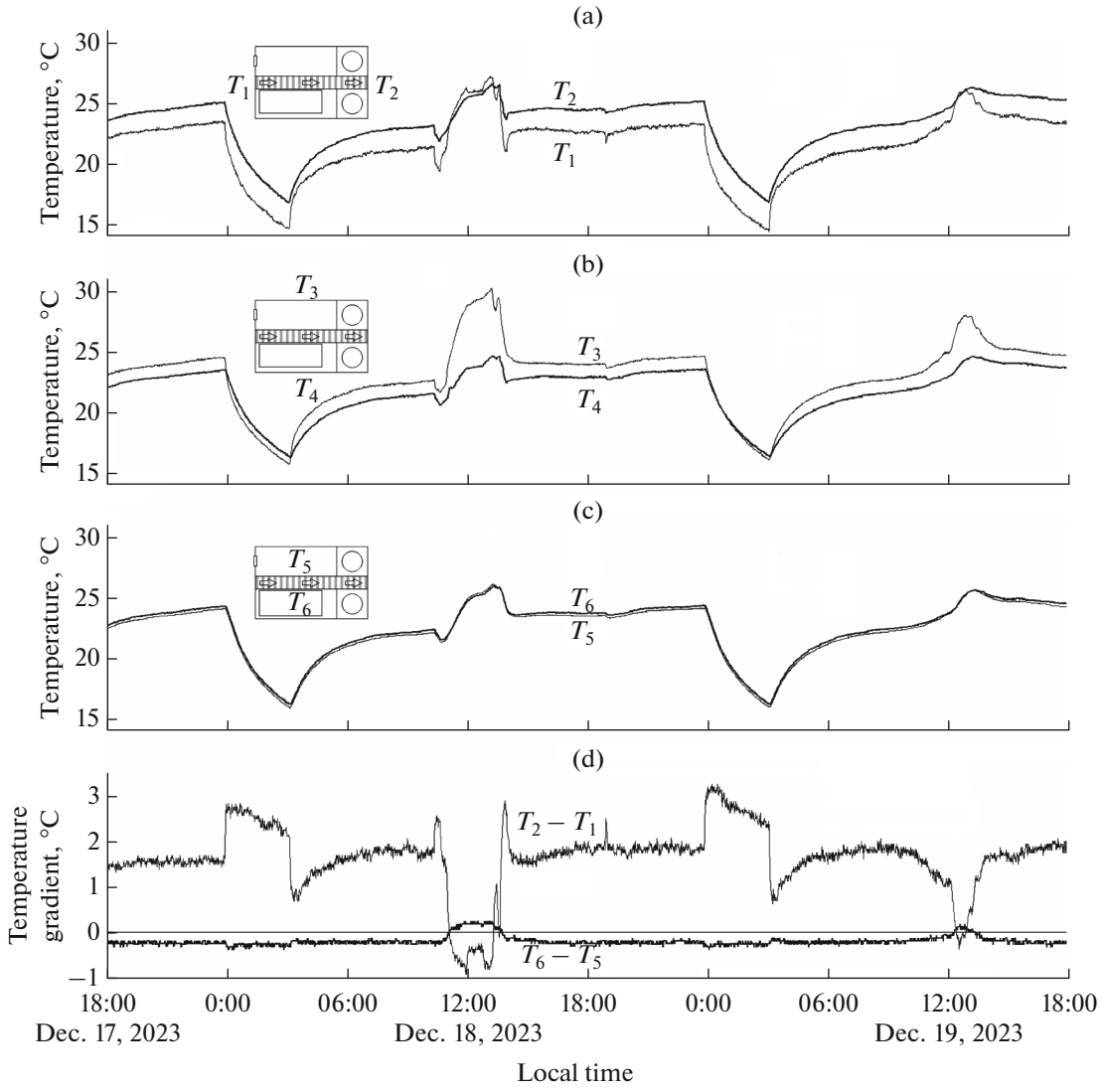

Fig. 6. Temperature and temperature gradient during lidar stability tests: (a) airflow temperature at the entrance T_1 (gray curve) and exit T_2 (bold curve) of the optical bench; (b) temperature of the top T_3 and bottom T_4 of the lidar casing; (c) temperature on the top T_5 and bottom T_6 of the optical bench; (d) temperature gradients $T_2 - T_1$ and $T_6 - T_5$.

FUNDING

This work was supported by the Ministry of Science and Higher Education of the Russian Federation (project no. 075-15-2021-934).

CONFLICT OF INTEREST

The authors of this work declare that they have no conflicts of interest.

REFERENCES

1. *Manual on Forecasting Meteorological Conditions for Aviation* (Gidrometeoizdat, Leningrad, 1985) [in Russian].
2. N. P. Shakina and A. R. Ivanova, *Forecasting Meteorological Conditions for Aviation* (TRIADA, Moscow, 2016) [in Russian].
3. Japan Aerospace Exploration Agency. www.aero.jaxa.jp/eng/research/star/safeavio/. Cited April 23, 2024.
4. www.oreanda.ru/en/transport/Boeing_and_JAXA_to_-Flight-test/article1173457/. Cited April 23, 2024.
5. Yu. A. Kravtsov and A. I. Saichev, "Effects of double passage of waves in randomly inhomogeneous media," Phys.-Uspekhi **25** (7), 494–508 (1982).
6. A. S. Gurvich, "Lidar sounding of turbulence based on the backscatter enhancement effect," Izv., Atmos. Ocean. Phys. **48** (6), 585–594 (2012).
7. I. A. Razenkov, "Engineering and technical solutions when designing a turbulent lidar," Atmos. Ocean. Opt. **35** (S1), 148–S158 (2022).

8. V. A. Kovalev and W. E. Eichinger, *Elastic Lidar: Theory, Practice, and Analysis Methods* (Wiley-IEEE, 2004).

9. *Lidar: Range-Resolved Optical Remote Sensing of the Atmosphere*, Ed. by C. Weitkamp (Springer, Berlin, 2005). https://doi.org/10.1007/b106786

10. V. V. Vorob'ev, "On the applicability of asymptotic formulas of retrieving "optical" turbulence parameters from pulse lidar sounding data: I—Equations," Atmos. Ocean. Opt. **30** (2), 156–161 (2017). https://doi.org/10.1134/S1024856017020142

11. I. A. Razenkov, "Turbulent lidar measurement technique and comparison with ground-based observations," Opt. Atmos. Okeana **37** (10), 874–882 (2024).

12. I. A. Razenkov, B. D. Belan, A. V. Mikhal'chishin, and G. A. Ivlev, "The use of the turbulent lidar for aviation safety," Atmos. Ocean. Opt. **37** (4), 492–501 (2024).